J|A|C|S ARTICLES

Published on Web 06/04/2009

Theoretical Analysis of the Individual Contributions of Chiral Arrays to the Chiroptical Properties of Tris-diamine Ruthenium Chelates

Yan Wang, Yuekui Wang,* Jianming Wang, Yang Liu, and Yitao Yang

Key Laboratory of Chemical Biology and Molecular Engineering of the Education Ministry, Institute of Molecular Science, Shanxi University, Taiyuan, Shanxi 030006, P. R. China

Received January 21, 2009; E-mail: ykwang@sxu.edu.cn

Abstract: Calculations of the excitation energies, oscillator and rotational strengths, and the CD spectra of 16 diastereoisomers of the tris-diamine ruthenium chelates $[Ru(en)_3]^{2+}$, $[Ru(pn)_3]^{2+}$, and $[Ru(bn)_3]^{2+}$ have been performed at the TDDFT/B3LYP/LanL2DZ+6-31G* level including solvent effects. The individual contributions of the chiral arrays, Δ/Λ octahedral core, δ/λ twists of the ligand rings, and *R*/*S* chiral carbons to the rotational strengths of related transitions have been quantitatively determined and graphically presented. It was found that the three chiral arrays Δ, δ and *S* each make their contributions to the CD spectra of the chelates with the sign alternated between negative and positive from long wavelength to short, but the intensities of the extrema are different for different chiral arrays. By simply combining the contributions of related chiral arrays in the chelates, all CD spectra of the 16 isomers obtained at the TDDFT level can be well reproduced, and those of the other conformers can also be well predicted, as expected. These findings not only make it possible to determine the absolute configurations and conformations of related chelates in solution from their CD spectra but also provide a deep insight into the chiroptical properties of the chelates.

Introduction

Since Werner first proposed the chiral tris-chelate structure for six-coordinate complexes with bidentate chelating ligands,[1,2] it has been apparent that combination of achiral metal and ligand components can generate chiral assemblies. Such chelates usually possess not only an overall dissymmetrical structure but also some locally chiral centers or arrays. In these, the irreducible chiral assembling units or *chiral arrays*, such as the Δ/Λ configurations at the octahedral core, the *R*/*S* carbon atoms at the methyl-substituted ligand ring, the δ/λ twists of the rings,[3] etc., have been expected to be responsible for the chiroptical properties of such chelates. To reveal the relationships between the chiroptical properties and molecular structures, much work has been done both experimentally and theoretically. Some empirical or semiempirical regional rules[4] for relating the position of substitution to the sign of lowest-energy *d*-electron optical activity in chiral complexes were obtained early in 1960s. However, no overall pictures for the individual contributions of different chiral arrays to the circular dichroism (CD) spectra of chiral molecules were established because of the difficulty in quantitatively calculating CD spectra during that time. In recent decades, however, with the development of density functional theory (DFT) and especially the improvement of time-dependent density functional theory (TDDFT),[5] properties of excited states for larger molecules can be calculated at the first principle level with good accuracy.[6−8] This makes it possible to perform such an analysis, as proposed and demonstrated by Wang[9] et al. in 2002. For this reason, the optical and chiroptical properties of some well-studied transition metal complexes also have been explored recently by Ziegler's group[10−13] using the TDDFT method.

As far as ruthenium complexes are concerned, most work focused on their special properties, such as luminescence, catalysis, and anticancer activities.[14−17] Some theoretical calculations of the CD spectra of ruthenium diimine complexes

(1) Werner, A. *Ber.* **1911**, *44*, 1887–1898.
(2) Werner, A. *Ber.* **1914**, *47*, 3087–3094.
(3) Herrero, S.; Usón, M. A. *Dalton Trans.* **2008**, *37*, 4993–4998.
(4) Mason, S. F. *Molecular Optical Activity and the Chiral Discriminations*; Cambridge University Press: Cambridge, 1982; pp 116−137.
(5) Marques, M. A. L.; Gross, E. K. U. *Annu. Rev. Phys. Chem.* **2004**, *55*, 427–455.
(6) Dreuw, A.; Head-Gordon, M. *Chem. Rev* **2005**, *105*, 4009–4037.
(7) Voloshina, E. N.; Wang, Y.; Voloshina, N. A.; Raabe, G.; Gais, H. J.; Fleischhauer, J. *Z. Naturforsch.* **2003**, *58A*, 443–450.
(8) Wang, Y.; Raabe, G.; Repges, C.; Fleischhauer, J. *Int. J. Quantum Chem.* **2003**, *93*, 265–270.
(9) Wang, Y.; Fleischhauer, J.; Bausch, S.; Sebestian, M.; Laur, P. H. *Enantiomer* **2002**, *7*, 343–374.
(10) Fan, J.; Ziegler, T. *Chirality* **2008**, *20*, 938–950.
(11) Jorge, F. E.; Autschbach, J.; Ziegler, T. *J. Am. Chem. Soc.* **2005**, *127*, 975–985.
(12) Jorge, F. E.; Autschbach, J.; Ziegler, T. *Inorg. Chem.* **2003**, *42*, 8902–8910.
(13) Autschbach, J.; Ziegler, T.; Jorge, F. E. *Inorg. Chem.* **2003**, *42*, 2867–2877.
(14) Hotze, A C. G.; Faiz, J. A.; Mourtzis, N.; Pascu, G. I.; Webber, P. R. A.; Clarkson, G. J.; Yannakopoulou, K.; Pikramenou, Z.; Hannon, M. J. *Dalton Trans.* **2006**, 3025–3034.
(15) Bernhard, S.; Barron, J. A.; Houston, P. L.; Abruña, H. D.; Ruglovksy, J. L.; Gao, X.; Malliaras, G. G. *J. Am. Chem. Soc.* **2002**, *124*, 13624–13628.
(16) Morilla, M. E.; Rodríguez, P.; Belderrain, T. R.; Graiff, C.; Tiripicchio, A.; Nicasio, M. C.; Pérez, P. Z. *Inorg. Chem.* **2007**, *46*, 9405–9414.
(17) Kostova, I. *Curr. Med. Chem.* **2006**, *13*, 1085–1107.

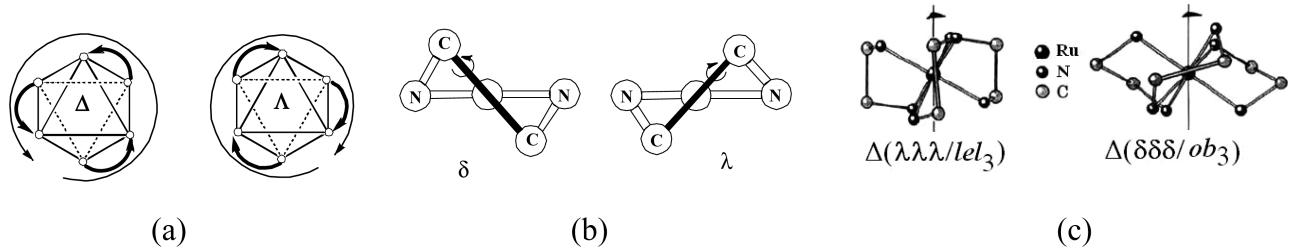

Figure 1. Configurational/conformational chirality and spatial disposition of the ligands: (a) Δ and Λ enantiomers of the octahedral core; (b) δ and λ twists of the five-membered ring; (c) *lel* and *ob* orientations of the ligands.

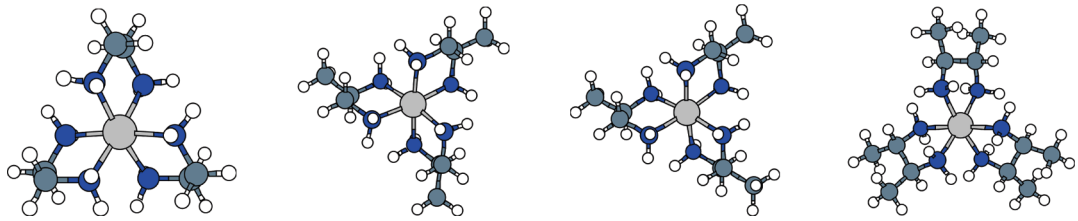

Figure 2. Most stable stereoisomers of the three kinds of chelates obtained at the DFT/B3LYP/LanL2DZ+6-31G* level (see Table 2 for details).

have been also reported,[18,19] but no analysis for the individual contributions of the chiral arrays was made.

In this paper, we shall present and discuss calculations of the optically active divalent ruthenium chelates. The main object of this research is to quantitatively assess the individual contributions of the Δ/Λ, *R*/*S*, and δ/λ steric arrangements to the CD spectra using the method proposed in ref 9 in order to gain a deep insight into the correlation of chiroptical properties with the stereochemistry of such systems.

To achieve this, the three kinds of tris-diamine ruthenium chelates, $[Ru(en)_3]^{2+}$, $[Ru(pn)_3]^{2+}$, and trans-$[Ru(bn)_3]^{2+}$ (en = ethylenediamine, pn = propane-1,2-diamine, bn = butane-2,3-diamine), have been taken into consideration. These compounds, which incorporate three nonplanar five-membered rings Ru(NC-CN) in a propeller-like disposition, display both configurational and conformational chirality, i.e., the Δ/Λ octahedral core, the δ/λ twists of the five-membered rings, and the *R*/*S* carbon atoms of the ligand rings, as depicted in Figure 1. The alternative notations *lel*/*ob* used in Figure 1c denote the para*lel* or *ob*lique orientation of the C−C bond of the ligand rings relative to the 3-fold or pseudo-3-fold axis of symmetry of the molecule.

Stereoisomers of the Chelates. Since the CD spectra of each pair of enantiomers have the same magnitude but are opposite in sign, calculations will be restricted to the Δ-configuration only, as the CD of the Λ-enantiomer can be generated simply by a mirror operation. In addition, a detailed conformational analysis[20] showed that only the stereoisomers with all half-chair conformations of the ligands are energetically favorable. Therefore, only these structures will be treated here.

For the $[Ru(en)_3]^{2+}$ chelates with a Δ-octahedral core, combination of δ/λ twists of the three ligand rings yields four diastereoisomers: $D_3\Delta(\lambda\lambda\lambda/lel_3)$, $C_2\Delta(\lambda\lambda\delta/lel_2ob)$, $C_2\Delta(\lambda\delta\delta/lelob_2)$ and $D_3\Delta(\delta\delta\delta/ob_3)$.

For the $[Ru(pn)_3]^{2+}$ chelates, combinations of δ/λ twists and *R*/*S* carbons will yield many more conformers. In order to limit the number of conformers to be treated, it will be assumed that all three ligand rings of each isomer exhibit the same twist sense, i.e., lel_3 or ob_3, although in solution some lel_2ob conformers will also be present at equilibrium, with both equatorial and axial substituents. Under this restriction, only the following eight diastereoisomers will therefore be included in the discussions: $C_3\Delta(R_e)(\lambda\lambda\lambda/lel_3)$, $C_3\Delta(S_a)(\lambda\lambda\lambda/lel_3)$, $C_3\Delta(R_a)(\delta\delta\delta/ob_3)$, $C_3\Delta(S_e)(\delta\delta\delta/ob_3)$, $C_1\Delta(R_e)(\lambda\lambda\lambda/lel_3)$, $C_1\Delta(S_a)(\lambda\lambda\lambda/lel_3)$, $C_1\Delta(R_a)$-$(\delta\delta\delta/ob_3)$, and $C_1\Delta(S_e)(\delta\delta\delta/ob_3)$, where the subscript "e" or "a" indicates the presence of equatorial or axial methyl substituents, respectively, at the three ligand carbon atoms with absolute configuration *R* or *S*, and the notation (R_e) is an abbreviation of ($R_eR_eR_e$) for simplicity. In addition, the isomers of C_1 symmetry are different from those of C_3 symmetry in the spatial disposition of the three ligands, as schematically illustrated in Figure 2.

For the $[Ru(bn)_3]^{2+}$ chelates, only the four diastereoisomers with D_3 symmetry will be considered here: $D_3\Delta(R_e,R_e)(\lambda\lambda\lambda/lel_3)$, $D_3\Delta(S_a,S_a)(\lambda\lambda\lambda/lel_3)$, $D_3\Delta(R_a,R_a)(\delta\delta\delta/ob_3)$ and $D_3\Delta(S_e,S_e)$-$(\delta\delta\delta/ob_3)$. This is sufficient for our purposes.

Computational Scheme. The ground-state energy calculations and geometry optimizations of the 16 Δ-diastereoisomers were performed employing the DFT method, as implemented in Gaussian03,[21] with the B3LYP functional and LanL2DZ+6-31G* mixed basis set (LanL2DZ[22,23] for Ru and 6-31G* for other atoms). The excitation energies, oscillator, and rotational strengths of the 50 lowest-lying singlet excited states were then calculated using the TDDFT method with the same functional and basis set. In all cases, solvent (water) effects have been included using the polarizable continuum model (PCM).[24]

The calculation of CD spectra and the analysis method of the individual contributions of the chiral arrays to the CDs of the chelates will be described in detail later.

Results and Discussions

Optimized Geometry Parameters. The geometry parameters of the 16 Δ-diastereoisomers optimized at the DFT/B3LYP/

(18) Guennic, B. L.; Hieringer, W.; Görling, A.; Autschbach, J. *J. Phys. Chem. A* **2005**, *109*, 4836–4846.
(19) Gorelsky, S. I.; Lever, A. B. P. *J. Organomet. Chem.* **2001**, *635*, 187–196.
(20) Corey, E. J.; Bailar, J. C. *J. Am. Chem. Soc.* **1959**, *81*, 2620–2629.
(21) *Gaussian 03, Revision E.01*; Frisch M. J., et al. Gaussian, Inc.: Wallingford, CT, 2004.
(22) Dunning, T. H., Jr.; Hay, P. J. In *Modern Theoretical Chemistry*; Schaefer, H. F., III., Ed.; Plenum: New York, 1976; Vol. 3, pp 1−28.
(23) Hay, P. J.; Wadt, W. R. *J. Chem. Phys.* **1985**, *82*, 270–283.

Table 1. Comparison of Calculated and Observed Structural Parameters of Isomer $[Ru(en)_3]^{2+}$ $C_2\Delta(\lambda\lambda\delta/lel_2ob)$[a]

parameters	gas phase	solution	crystal[25]
Ru−N	2.1997	2.1818	2.129
C−N	1.4989	1.4904	1.475
C−C	1.5202	1.5214	1.491
C−H	1.0952	1.0968	
N−H	1.0227	1.0278	
N−Ru−N	106.65	106.77	106.8
N−C−C	109.09	108.96	109.9
C−N−Ru−N	16.06	15.73	15.6
C−C−N−Ru	13.77	14.23	14.9
N−C−C−N	−18.61	−19.39	−20.2

[a] Bond lengths are in angstroms; bond angles and dihedral angels in degrees.

Table 2. Relative Energies of the Three Kinds of Ruthenium Chelates (kcal/mol)

		energies	
chelates	stereochemistry	without zero-point energy correction	with zero-point energy correction
$Ru(en)_3$	$D_3\Delta(\lambda\lambda\lambda/lel_3)$	0.000	0.000
	$C_2\Delta(\lambda\lambda\delta/lel_2ob)$	0.800	0.873
	$C_2\Delta(\lambda\delta\delta/lelob_2)$	0.985	1.051
	$D_3\Delta(\delta\delta\delta/ob_3)$	1.010	1.302
$Ru(pn)_3$	$C_3\Delta(R_e)(\lambda\lambda\lambda/lel_3)$	0.000	0.000
	$C_3\Delta(S_e)(\delta\delta\delta/ob_3)$	0.778	1.015
	$C_3\Delta(S_a)(\lambda\lambda\lambda/lel_3)$	9.740	10.319
	$C_3\Delta(R_a)(\delta\delta\delta/ob_3)$	10.697	11.713
	$C_1\Delta(R_e)(\lambda\lambda\lambda/lel_3)$	0.000	0.000
	$C_1\Delta(S_e)(\delta\delta\delta/ob_3)$	0.367	0.573
	$C_1\Delta(S_a)(\lambda\lambda\lambda/lel_3)$	9.510	10.235
	$C_1\Delta(R_a)(\delta\delta\delta/ob_3)$	10.826	11.719
$Ru(bn)_3$	$D_3\Delta(S_e,S_e)(\delta\delta\delta/ob_3)$	0.000	0.000
	$D_3\Delta(R_e,R_e)(\lambda\lambda\lambda/lel_3)$	0.284	0.306
	$D_3\Delta(S_a,S_a)(\lambda\lambda\lambda/lel_3)$	21.024	21.816
	$D_3\Delta(R_a,R_a)(\delta\delta\delta/ob_3)$	22.093	23.210

LanL2DZ+6-31G* level in aqueous solution are listed in Supporting Information. A short comparison of the optimized and observed[25] structural parameters for the $C_2\Delta(\lambda\lambda\delta/lel_2ob)$ stereoisomer of $[Ru(en)_3]^{2+}$ chelate is given in Table 1. Since the parameters obtained in solution are much closer to the crystal data than those in the gas phase, our discussions below will refer to the solution structures of the chelates except as otherwise stated.

Relative Ground-State Energy. The relative ground-state energies for fully optimized structures of the 16 diastereoisomers in aqueous solution are listed in Table 2.

The relative stability sequences of the isomers are therefore as follows (without entropy corrections):

$$[Ru(en)_3]^{2+}: D_3\Delta lel_3 > C_2\Delta lel_2ob > C_2\Delta lelob_2 \approx D_3\Delta ob_3$$

$$[Ru(pn)_3]^{2+}: C_3\Delta(R_e)lel_3 > C_3\Delta(S_e)ob_3 \gg C_3\Delta(S_a)lel_3 > C_3\Delta(R_a)ob_3$$

$$C_1\Delta(R_e)lel_3 > C_1\Delta(S_e)ob_3 \gg C_1\Delta(S_a)lel_3 > C_1\Delta(R_a)ob_3$$

$$[Ru(bn)_3]^{2+}: D_3\Delta(S_e,S_e)ob_3 \approx D_3\Delta(R_e,R_e)lel_3 \gg D_3\Delta(S_a,S_a)lel_3 > D_3\Delta(R_a,R_a)ob_3$$

However, if the entropy effects are taken into consideration, the stability sequences of the isomers for $[Ru(en)_3]^{2+}$ will become $D_3\Delta lel_3 > C_2\Delta lel_2ob > C_2\Delta lelob_2 > D_3\Delta ob_3$, because the statistical weight of $C_2\Delta lelob_2$ is 3 times that of $D_3\Delta ob_3$. For chelates $[Ru(pn)_3]^{2+}$ and $[Ru(bn)_3]^{2+}$, the isomers with methyl groups at equatorial positions (e) are much preferred compared with those at axial positions (a).

DFT Energy Levels and Kohn−Sham Orbitals. The calculated DFT energy levels for the ground states of the 16 Δ-diastereoisomers are displayed in Figure 3. The corresponding Kohn−Sham (KS) orbitals can be found in Supporting Information. Some KS orbitals for the $D_3\Delta(\lambda\lambda\lambda/lel_3)$ isomer of $[Ru(en)_3]^{2+}$ chelate are illustrated in Figure 4.

The DFT energy levels are separated into four groups by three considerable energy gaps: two groups for the unoccupied levels and two for the occupied levels. This grouped distribution of the energy levels determines the excitation properties of the chelates and leads to relative simple CD/UV spectra down to 180 nm also, as will be seen later.

Detailed analyses on the corresponding KS orbitals show that, in all cases, the highest three occupied orbitals are dominated by the *d* atomic orbitals of the central ion Ru(II). The next several occupied orbitals, e.g., the 53rd orbital in Figure 4, are mainly *n*-orbitals occupied by the lone-pair electrons of the nitrogen atoms with some delocalized π-character. The other occupied orbitals are all σ-type, mainly located on the Ru−N and C−C bonds. Interestingly, the lowest three unoccupied orbitals are some Rydberg 5*p*-like $\sigma^*_{N\text{-}H/C\text{-}H}$ orbitals, while the next two are the normal *d*-like $\sigma^*_{Ru\text{-}N}$ orbitals, which are significantly higher than the formers in energy. The other unoccupied orbitals are all σ*-types involving the central ion Ru(II) partly or significantly.

In addition, the splitting pattern of the DFT energy levels around the HOMO and LUMO can be well understood according to perturbation theory.[26] Initially, the 5-fold degenerate *d*-level of the central ion Ru(II) is split into one occupied 3-fold degenerate level ($\boldsymbol{t}_2$) and one unoccupied 2-fold degenerate level ($\boldsymbol{e}$) under the perturbation of the six ligating nitrogen atoms, which form an approximately octahedral core with a symmetry group O. Depending on the full symmetry of isomers, the occupied $\boldsymbol{t}_2$ level is further split into two (for D_3 and C_3 symmetries) or three (for C_2 and C_1 symmetries) levels (cf. Figure 5) as a result of perturbations of the other atoms in the molecules. Similarly, the unoccupied $\boldsymbol{e}$ level is split into two levels for the C_2 and C_1 symmetries but remains doubly degenerate for the D_3 and C_3 symmetries. In the case of $[Ru(en)_3]^{2+}$ chelate, for example, the occupied $\boldsymbol{t}_2$ level is split into two levels, $11\boldsymbol{a}_1$ and $19\boldsymbol{e}$, for the isomer $D_3\Delta(\lambda\lambda\lambda/lel_3)$ and three levels, $28\boldsymbol{b}$, $29\boldsymbol{a}$ and $30\boldsymbol{a}$ for the isomer $C_2\Delta(\lambda\lambda\delta/lel_2ob)$. See Figure 5 for a detailed energy level correlation diagram.

Rotational Strengths and Transition Moments. The excitation energies, oscillator and rotational strengths (both in length and velocity forms), as well as the electric and magnetic transition dipole moments for the 50 lowest energy transitions of the 16 diastereoisomers were obtained using the TDDFT method and the optimized geometries. Part of the results for the conformer $D_3\Delta(\lambda\lambda\lambda/lel_3)$ of $[Ru(en)_3]^{2+}$ are listed in Table 3; more results can be found in Supporting Information. As the rotational strengths calculated in velocity form are independent of the

(24) Mennucci, B.; Tomasi, J.; Cammi, R.; Cheeseman, J. R.; Frisch, M. J.; Devlin, F. J.; Gabriel, S.; Stephens, P. J. *J. Phys. Chem. A* **2002**, *106*, 6102–6113.
(25) Smolenaers, P. J.; Beattie, J. K.; Hutchinson, N. D. *Inorg. Chem.* **1981**, *20*, 2202–2206.
(26) McWeeny, R. *Methods of Molecular Quantum Mechanics*; Academic Press Inc.: London, 1992; pp 285−324.

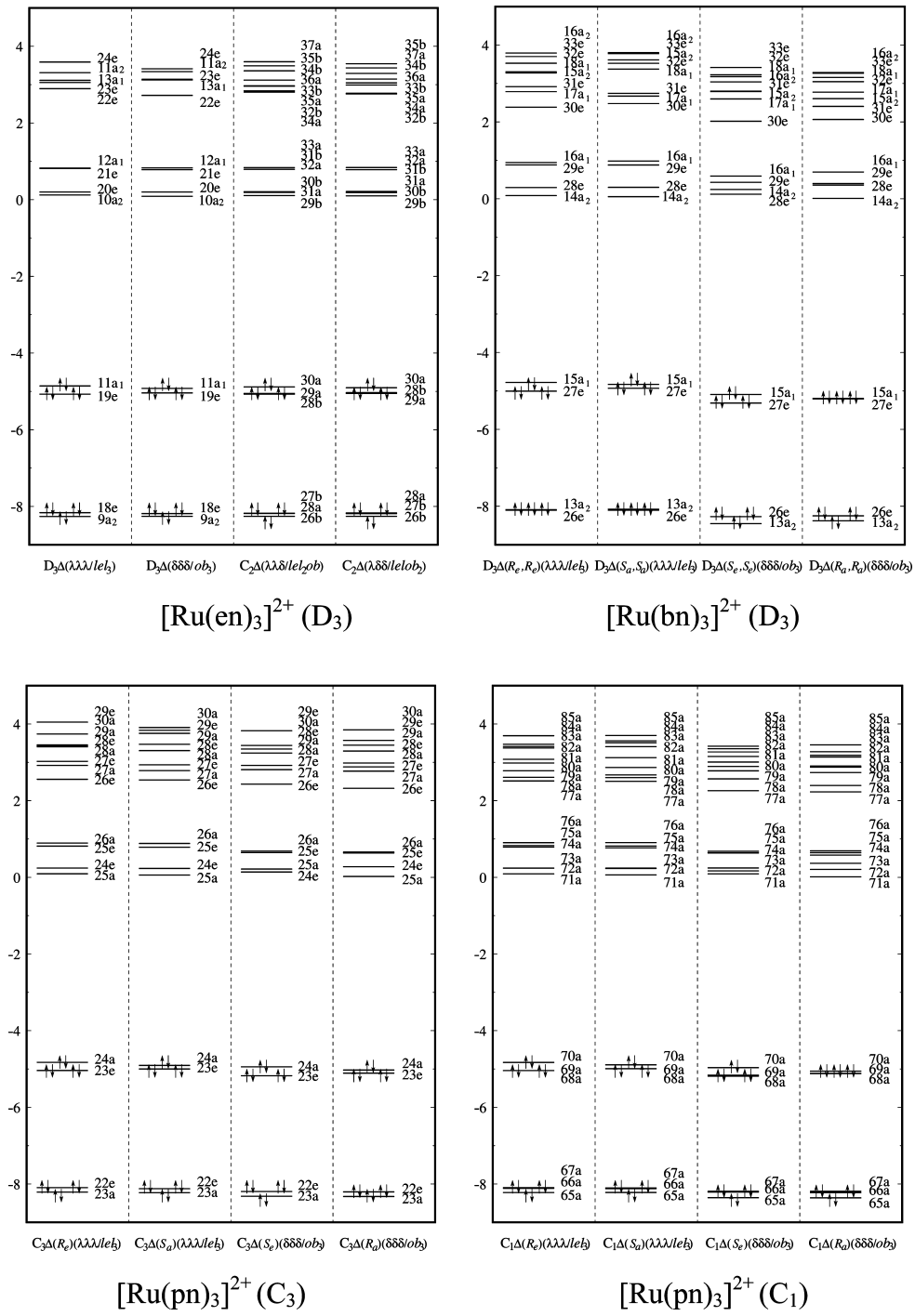

Figure 3. DFT energy levels of the ruthenium chelates (energy in eV).

choice of origin, only this form will be addressed below, although no significant difference between the two forms was observed.

Analysis of the results reveals the significant characteristics that all transitions with $\lambda > 170$ nm are mainly originated from the three highest occupied *d*-levels. In most cases, the three lowest energy transitions are the typical magnetic dipole allowed *d*-*d* transitions, followed by several weak Rydberg 5*p*-like *d*-$\sigma^*_{N-H/C-H}$ transitions and a stronger *d*-σ^*_{N-H} transition $1^1A_1 \rightarrow 6^1E$ with significant charge-transfer (M $\rightarrow$ L) character. The Rydberg-like transitions can be observed in the gas phase and sometimes in solid states but may not be clearly observed in solutions due to the rapid electronic relaxation with consequent line broadening. This solvent effect could be partly simulated by use of the Gaussian curves with larger band widths.

CD and UV Spectra. The CD and UV spectra of the 16 diastereoisomers were generated as a sum of Gaussians, centered at the calculated wavelengths λ_{calc} with integral intensities proportional to the rotational (for CD) or oscillator (for UV) strengths of the corresponding transitions. The half bandwidth Γ at ε_{max}/e of the Gaussians were generated using the empirical formula[27] $\Gamma = k\lambda_{cal}^{1.5}$, where λ_{cal} is the calculated transition

(27) Kurapkat, G.; Krüger, P.; Wollmer, A.; Fleischhauer, J.; Kramer, B.; Zobel, E.; Koslowski, A.; Woody, R. W. *Biopolymers* **1997**, *41*, 267–287.

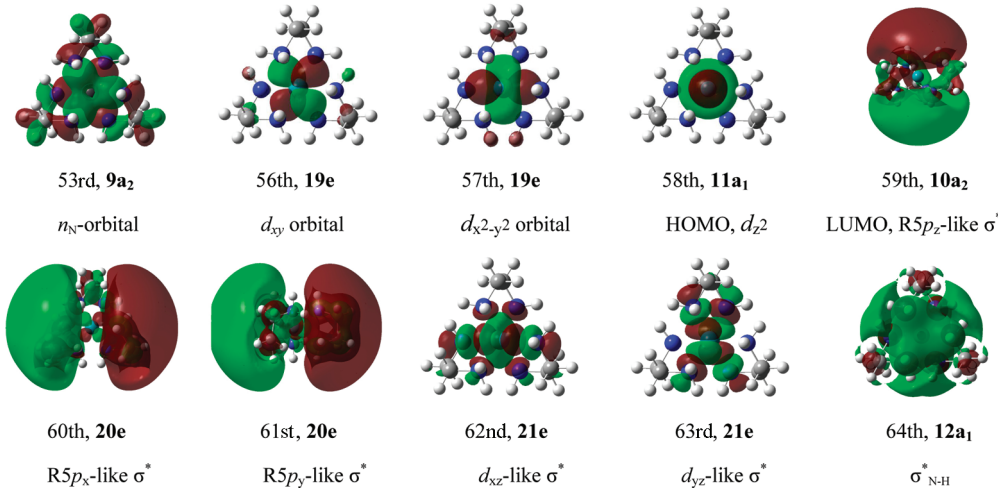

Figure 4. Kohn−Sham orbitals of the isomer $D_3\Delta(\lambda\lambda\lambda/lel_3)$ of $[Ru(en)_3]^{2+}$, where R means Rydberg.

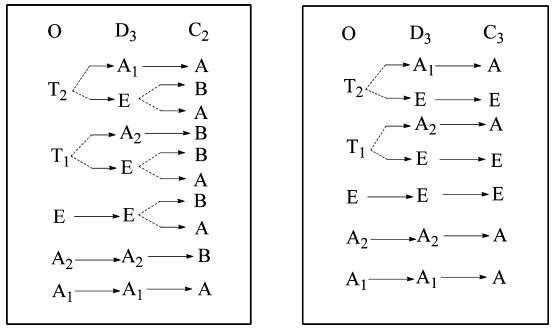

Figure 5. Energy level correlation diagram in different symmetry fields.

wavelength and the parameter k has been assumed to be 4.81×10^{-3} (which yields $\Gamma = 25$ nm for an absorption band at $\lambda = 300$ nm) to best reproduce the experimental spectra[28] of $[Ru(en_3)]^{2+}$. The resulting CD spectra are shown in Figure 6, which exhibit the following striking characteristics.

In the long-wavelength region of 280−460 nm, all of the $\Delta(\lambda\lambda\lambda)$ conformers display a bell-shaped dominant CD band with negative tails on both sides. In these, the dominant positive band around 360 nm is a typical *d-d* absorption band due to the transition $^1A \rightarrow {}^1A_2$ ($d_{x2-y2},d_{xy} \rightarrow d_{xz},d_{yz}$). The long-wavelength tail at about 406 nm is a less stronger CD band resulting from the transition $^1A_1 \rightarrow {}^1E$ ($d_{z2} \rightarrow d_{xz},d_{yz}$), while the short-wavelength tail at about 314 nm is very weak, which arises from the transitions $^1A_1 \rightarrow {}^2E$ ($d_{x2-y2},d_{xy} \rightarrow d_{xz},d_{yz}$). In the short-wavelength region, there is a strong positive CD band at about 254 nm, which is dominated by the charge transfer (CT) transition $^1A_1 \rightarrow {}^6E$ ($d_{xy},d_{x2-y2} \rightarrow \sigma^*_{N-H}$), mixed with some Rydberg-like transitions $^1A_1 \rightarrow {}^2A_2,{}^4E$ ($d_{z2},d_{x2-y2},d_{xy} \rightarrow R5p_z$) and $^1A_1 \rightarrow {}^3E,{}^3A_2,{}^5E$ ($d_{z2},d_{x2-y2},d_{xy} \rightarrow R5p_x,5p_y$).

In addition, all of the $\Delta(\delta\delta\delta)$ conformers show a negative CD band and a positive one with different amplitudes. The negative band at about 394 nm is dominated by the *d-d* transition $^1A_1 \rightarrow {}^1E$ ($d_{z2} \rightarrow d_{xz},d_{yz}$), significantly mixed with the contributions of $^1A \rightarrow {}^1A_2,{}^2E$ ($d_{x2-y2},d_{xy} \rightarrow d_{xz},d_{yz}$). The positive band around 280 nm is also a mixed absorption band dominated by the Rydberg-like transitions $^1A_1 \rightarrow {}^2A_2,{}^3E$ ($d_{z2},d_{x2-y2},d_{xy} \rightarrow R5p_z$) and $^1A_1 \rightarrow {}^4E,{}^3A_2,{}^5E$ ($d_{z2},d_{x2-y2},d_{xy} \rightarrow R5p_x,5p_y$) and mixed with the CT transition $^1A_1 \rightarrow {}^6E$ ($d_{xy},d_{x2-y2} \rightarrow \sigma^*_{N-H}$).

For the conformers $\Delta(\lambda\lambda\delta)$ and $\Delta(\lambda\delta\delta)$, the band shapes of CD spectra in this range are transitional between those of the $\Delta(\lambda\lambda\lambda)$ and $\Delta(\delta\delta\delta)$ species, as expected.

The calculated UV spectra of the chelates (see Supporting Information) contain two bands: a weak *d-d* absorption band at about 378 nm and a stronger UV band around 263 nm.

On the basis of the above results, the observed CD spectrum (cf. Figure 7) for the $[Ru(en)_3]\cdot I_2$ chelate[28] can be interpreted. It contains a positive band with a maximum at 402 nm and two negative bands centered at 348 nm and 284 nm. The later band, at 284 nm, was guessed to be a charge-transfer band,[28] but no more information was found in literatures. According to our calculations, this guess can be partly confirmed because it involves a stronger charge-transfer (M → L) transition and several weak Rydberg like transitions. By assigning the first two bands to the *d-d* transitions from the ground state $^1A_1$ to excited states ^1E and $^1A_2$, respectively, Elsbernd and Beattie[28] could determine the absolute configuration of $[Ru(en)_3]^{2+}$ as $\Lambda(\delta\delta\delta/lel_3)$, which is the enantiomer of $\Delta(\lambda\lambda\lambda/lel_3)$. However, by inverting the sign of the calculated spectrum for $\Delta(\lambda\lambda\lambda/lel_3)$, the resulting CD curve is only qualitatively in agreement with the observed one as far as the wavelength ($\lambda_{cal} = 254$ nm, $\lambda_{obs} = 284$ nm) of the CT band is concerned. Since for other isomers with higher energies the calculated wavelengths of the CT band are around 280 nm, this means that not only the most stable conformer but also the less stable ones with the same octahedral core make their contributions to the observed CD.

As the inversion barrier of the octahedral core is very high, a statistically averaged CD spectrum has been calculated as a sum of the CD curves of the four isomers, $\Delta(\lambda\lambda\lambda/lel_3)$, $\Delta(\lambda\lambda\delta/lel_2ob)$, $\Delta(\lambda\delta\delta/lelob_2)$ and $\Delta(\delta\delta\delta/ob_3)$, weighted by the Boltzmann factors 0.3958, 0.1024 × 3, 0.0750 × 3, and 0.0719, respectively. These factors were obtained using the formula $g_j = w_j \exp(-\Delta\varepsilon_j/kT)/\Sigma_{i=1}^{4} w_i \exp(-\Delta\varepsilon_i/kT)$ at room temperature, with $\Delta\varepsilon_i$ being the relative energies of the four structures, and w_i, the statistical weights: 1, 3, 3, 1. Since the final CD spectra calculated using the relative energies with or without zero-point energy corrections are almost identical, only the latter has been converted into that of the Λ-enantiomers and displayed in Figure 7(b).

Generally speaking, the averaged CD curve is in good agreement with the observed one, except that there is a weak

(28) Elsbernd, H.; Beattie, J. K. *Inorg. Chem.* **1969**, *8*, 893–899.

Table 3. Oscillator Strengths, Rotational Strengths, and Transition Moments of $[Ru(en)_3]^{2+}$ $D_3\Delta(\lambda\lambda\lambda/lel_3)^{\dagger}$

sym	λ (nm)	f	R_{vel} (DBM)	μ (Debye)		m (BM)		assignments
1*E*	382.73	0.0000	−0.1042	−0.0264	x	1.7188	x	$d_{z2} \rightarrow d_{yz}$
								$d_{x2\text{-}y2},d_{xy} \rightarrow d_{xz},d_{yz}$
		0.0000	−0.1042	0.0264	y	−1.7188	y	$d_{z2} \rightarrow d_{xz}$
								$d_{x2\text{-}y2},d_{xy} \rightarrow d_{xz},d_{yz}$
$1A_2$	368.06	0.0002	0.2441	0.1172	z	1.8147	z	$d_{x2\text{-}y2},d_{xy} \rightarrow d_{xz},d_{yz}$
2*E*	314.48	0.0000	−0.0278	0.0574	x	−0.2570	x	$d_{z2} \rightarrow d_{yz}$
								$d_{x2\text{-}y2},d_{xy} \rightarrow d_{xz},d_{yz}$
		0.0000	−0.0278	−0.0574	y	0.2570	y	$d_{z2} \rightarrow d_{xz}$
								$d_{x2\text{-}y2},d_{xy} \rightarrow d_{xz},d_{yz}$
$2A_2$	296.67	0.0005	0.0190	0.1754	z	0.0379	z	$d_{z2} \rightarrow R5p_z$
3*E*	287.85	0.0003	−0.0035	−0.1337	x	0.1952	x	$d_{z2} \rightarrow R5p_x$
		0.0003	−0.0035	−0.1337	y	0.1952	y	$d_{z2} \rightarrow R5p_y$
4*E*	281.54	0.0000	−0.0011	−0.0386	x	0.0519	x	$d_{x2\text{-}y2} \rightarrow R5p_z$
		0.0000	−0.0011	0.0386	y	−0.0519	y	$d_{xy} \rightarrow R5p_z$
$3A_2$	274.27	0.0000	0.0254	0.0219	z	0.2422	z	$d_{x2\text{-}y2},d_{xy} \rightarrow R5p_x,5p_y$
5*E*	272.97	0.0008	0.0191	0.2107	x	0.0766	x	$d_{x2\text{-}y2} \rightarrow R5p_x$, $d_{xy} \rightarrow 5p_y$
		0.0008	0.0191	−0.2107	y	−0.0766	y	$d_{x2\text{-}y2} \rightarrow R5p_y$, $d_{xy} \rightarrow 5p_x$
6*E*	251.39	0.0080	0.0823	−0.6527	x	−0.1478	x	$d_{xy} \rightarrow \sigma^*_{N-H}$
		0.0080	0.0823	−0.6527	y	−0.1478	y	$d_{x2\text{-}y2} \rightarrow \sigma^*_{N-H}$
7*E*	180.42	0.0046	−0.0133	−0.4179	x	0.0314	x	$d_{z2} \rightarrow \sigma^*_{C-H/N-H}$
		0.0046	−0.0133	−0.4179	y	0.0314	y	$d_{z2} \rightarrow \sigma^*_{C-H/N-H}$
8*E*	177.74	0.0009	0.0079	−0.1848	x	−0.0455	x	$d_{z2} \rightarrow \sigma^*_{C-H}$
		0.0009	0.0079	0.1848	y	0.0455	y	$d_{z2} \rightarrow \sigma^*_{C-H}$
$4A_2$	174.96	0.0036	0.0038	0.3645	z	0.0125	z	$d_{x2\text{-}y2},d_{xy} \rightarrow \sigma^*_{C-H/N-H}$
9*E*	174.75	0.0290	−0.0033	1.0381	x	−0.0036	x	$d_{x2\text{-}y2},d_{xy} \rightarrow \sigma^*_{C-H/N-H}$
		0.0290	−0.0033	−1.0381	y	0.0036	y	$d_{x2\text{-}y2},d_{xy} \rightarrow \sigma^*_{C-H/N-H}$
$5A_2$	172.77	0.0014	−0.2081	0.2298	z	−0.4129	z	$d_{z2} \rightarrow \sigma^*_{N-H}$
								$d_{x2\text{-}y2},d_{xy} \rightarrow \sigma^*_{C-H}$
$6A_2$	172.04	0.0168	0.1397	0.7834	z	0.1858	z	$d_{z2} \rightarrow \sigma^*_{N-H}$
								$d_{x2\text{-}y2},d_{xy} \rightarrow \sigma^*_{C-H}$
10*E*	172.01	0.0031	−0.0407	−0.3386	x	0.1510	x	$d_{x2\text{-}y2},d_{xy} \rightarrow \sigma^*_{C-H}$
		0.0031	−0.0407	0.3386	y	−0.1510	y	$d_{x2\text{-}y2},d_{xy} \rightarrow \sigma^*_{C-H}$
11*E*	171.24	0.0025	−0.0823	−0.9552	x	0.1002	x	$d_{xy} \rightarrow \sigma^*_{N-H}$
		0.0025	−0.0823	−0.9552	y	0.1002	y	$d_{x2\text{-}y2} \rightarrow \sigma^*_{N-H}$

† The forbidden transitions to $^1A_1$ are not listed here. R5*p* means the Rydberg 5*p*-like $\sigma^*_{N-H/C-H}$ orbitals, not pure Rydberg 5*p*'s. Similarly, d_{xz} and d_{yz} indicate the two unoccupied d_{xz}- and d_{yz}-like σ^*_{Ru-N} orbitals, respectively.

positive peak at about 320 nm in the calculated spectrum, while the corresponding peak drops to the negative range in the observed one. This small discrepancy could be partly ascribed to the weakness[29] of TDDFT method for calculations of the CT and Rydberg-like transitions, and partly to the optimized bond lengths of Ru−N, which are a little bit longer than the measured ones. To clarify the latter problem, additional calculations have been done using partially optimized geometries with the bond lengths of Ru−N being fixed at 2.16 Å (about 0.02 Å shorter than the fully optimized geometries). The resulting Boltzmann-weighted CD curve is shown in Figure 7(c), which is clearly in better agreement with the observed one as far as the band shape is concerned.

Based on this agreement, we conclude that besides the most stable conformer $\Lambda(\delta\delta\delta/lel_3)$, the less stable ones $\Lambda(\delta\delta\lambda/lel_2ob)$, $\Lambda(\delta\lambda\lambda/lelob_2)$ also make considerable contributions to the CD spectrum observed in solution.

Since both results obtained using geometries optimized with or without the constraint are nearly identical except for their averaged CD, only the latter will be discussed below.

Contributions of the Chiral Arrays to CD Spectra. The chiroptical properties of a molecule are theoretically determined by the rotational strengths of related transitions in the molecule. According to the Wigner-Eckart theorem,[30] the rotational strength $R^{0n} = Im\{\langle\Psi_0|\hat{\boldsymbol{\mu}}|\Psi_n\rangle \cdot \langle\Psi_n|\hat{\boldsymbol{m}}|\Psi_0\rangle\}$ for given transition $\Psi_0 \rightarrow \Psi_n$ can be expressed as the product of a 'geometry' factor and a 'physical' part. The geometry factor is uniquely determined by the molecular symmetry, while the physical part depends on the detailed electronic structure of the molecule. In other words, for a given transition in different stereoisomers with the same molecular symmetry, the rotational strengths of the transition are different only in their physical part, because their geometry factors are identical.

Thus, if we assume that the rotational strength of a transition can be expressed as a sum of contributions each associated with one chiral array in the chelate, such contributions can then be determined from the rotational strengths of a given transition in different stereoisomers with the same molecular symmetry, as demonstrated in reference 9. For the chelates discussed here, only three parameters $\underline{\Delta}$, $\underline{\delta}$ and $\underline{R}$ are needed to represent the individual contributions of Δ-core, δ-twist and *R*-type carbon atom, respectively, because those contributions for objects constituting an enantiomeric pair of chiral arrays are exactly the same in magnitude but opposite in sign. The results are tabulated in Supporting Information and presented graphically in Figure 6 in the form of contributions to the CD curves.

Note that the sets of parameters $\underline{\Delta}$, $\underline{\delta}$, and $\underline{R}$ obtained above are both symmetry- and chelate-dependent but are independent of the conformers involved in deriving them, as displayed in Figures 8a−c; where the contribution of *R*-type carbon atom has been replaced by that of the *S*-type to facilitate later discussions.

(29) Diedrich, C.; Grimme, S. *J. Phys. Chem. A* **2003**, *107* (14), 2524–2539.

(30) Wigner, E. P. *Group Theory and Its Application to the Quantum Mechanics of Atomic Spectra*; Academic Press: New York, 1959; pp 131−257.

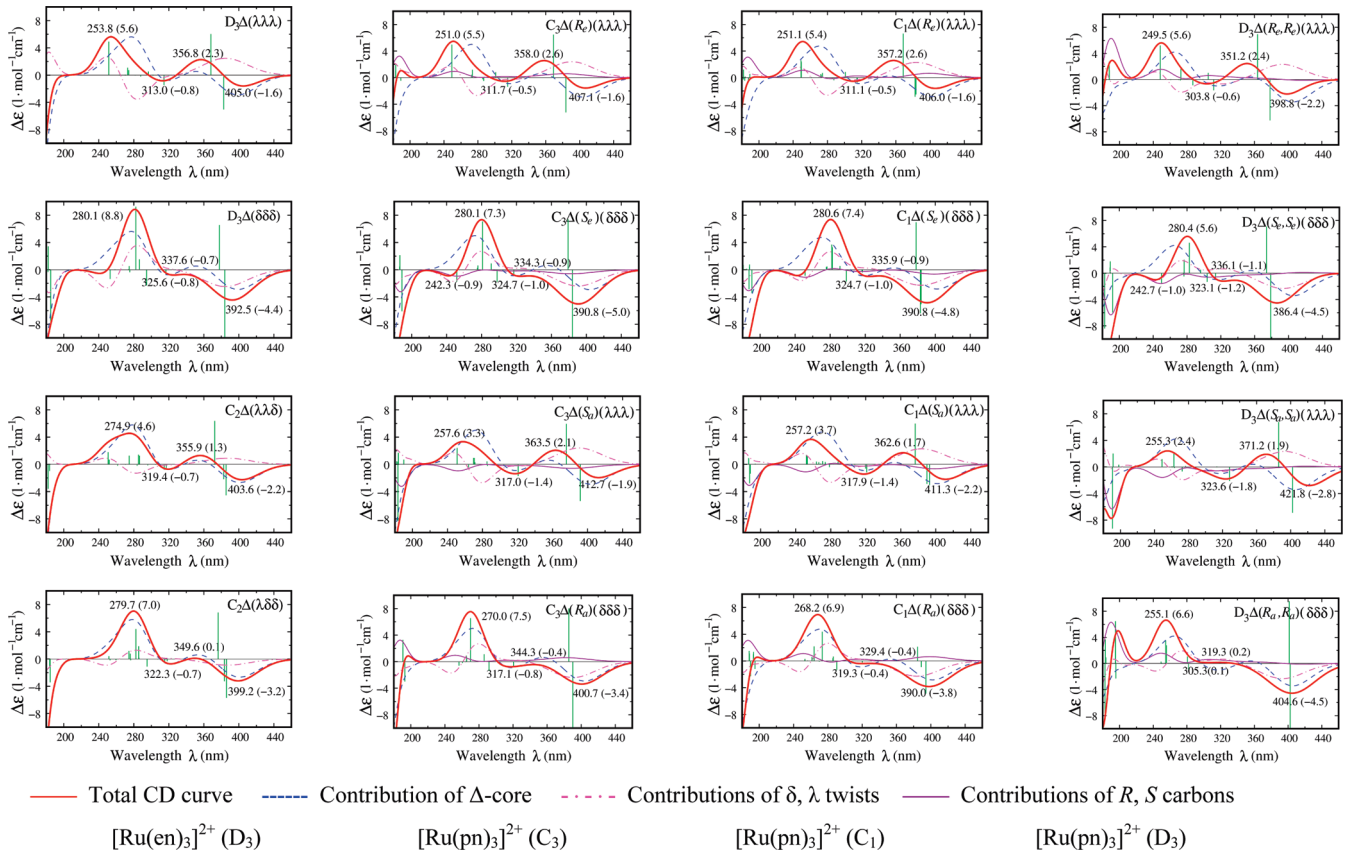

Figure 6. CD spectra of the 16 Δ-stereoisomers of ruthenium chelates.

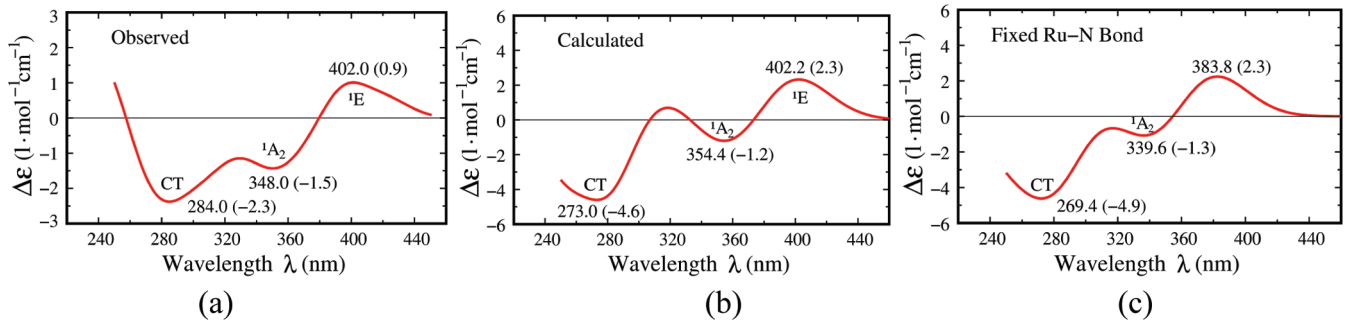

Figure 7. Comparison of the calculated and observed CD spectra of the Λ-$[Ru(en)_3]^{2+}$ configuaration: (a) observed CD; (b) calculated using optimized geometries; (c) calculated using partially optimized geometries with the bond lengths of Ru−N being fixed at 2.16 Å.

The first observation on the figure is that all contribution curves of the Δ-core, *δ*-twist, and *S*-type carbon mainly consist of four bands with the sign pattern alternated between negative and positive, although for the chelate $Ru[(bn)_3]^{2+}$ with D_3 symmetry the contribution of the *S*-type carbon atom shows an additional positive band around 417 nm, but which is too weak to be important. In addition, for the contribution of the Δ-core the sign of the second band at about 354 nm is very sensitive to the bond lengths of Ru−N due to the metal−ligand interactions in the octahedral core, as mentioned before. This fact together with the magnitudes of the contributions indicate that the dominant contributions arise from the influence of the Δ/Λ core configurations and less so from the *δ*/*λ* twists of the three five-membered ligand rings, while the contributions of any *R*/*S* chiral carbon atoms of the ligand rings are small.

Application of the Chiral Parameters. It is well-known that the chiroptical properties of a molecule strictly depend on the molecular structure and symmetry. Such being the case, one might ask what the potential usage of the chiral parameters is, besides their theoretical meaning mentioned above. In other words, since one usually expects the chiral arrays to be responsible for the chiroptical properties of such compounds, it is necessary to check at what levels this intuition-based concept could be confirmed.

Comparing the transition energies and the chiral parameters $\underline{\Delta}$, $\underline{\delta}$, and $\underline{R}$ of related transitions in chelates with different structures and different symmetries, we found that they are also closely related. This is manifest for transition energies according to the correlation diagram shown in Figure 5 but not so straightforward for parameters $\underline{\Delta}$, $\underline{\delta}$, and $\underline{R}$, because the transitions in chelates with different symmetries follow different selection rules. However, as far as the dominant transitions involved in the CD bands are concerned, they are both electrically and magnetically allowed for chelates with different symmetries, and the corresponding rotational strengths mostly depend on the types and the number of chiral arrays, as revealed

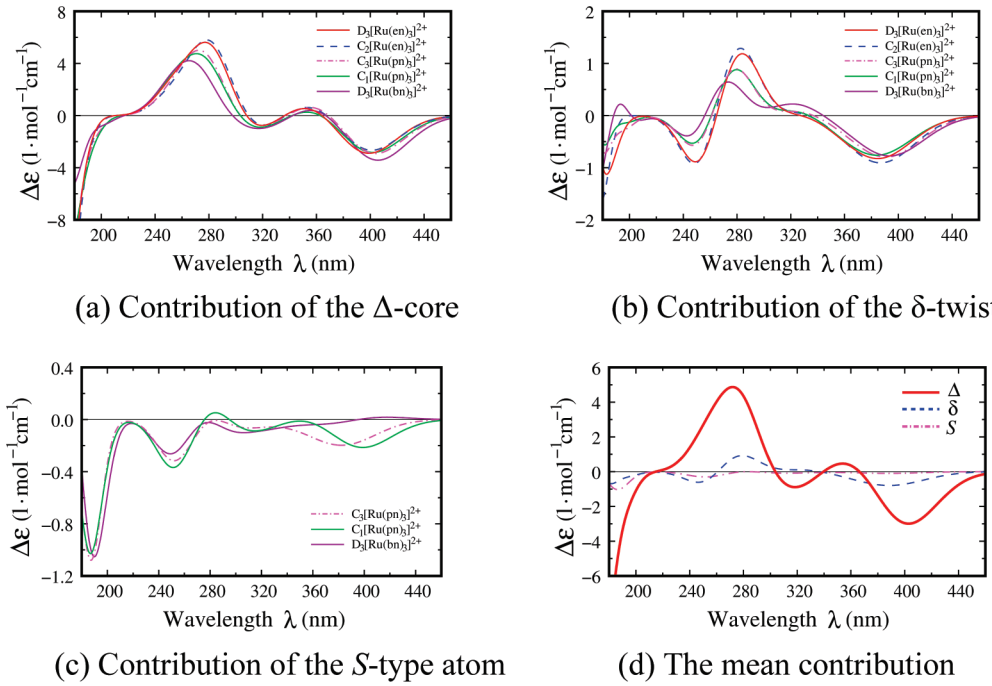

(a) Contribution of the Δ-core (b) Contribution of the δ-twist

(c) Contribution of the *S*-type atom (d) The mean contribution

Figure 8. Individual contributions of the chiral arrays to the CD spectra of different chelates.

Table 4. Mean Contributions of the Three Chiral Arrays to the Rotational Strengths

no.	sym	λ (nm)	$\underline{\Delta}$ (DBM)	$\underline{\delta}$ (DBM)	$\underline{R}$ (DBM)
1	1*E*	387.17	−0.3429	−0.0368	0.0043
2	2*A*	377.13	0.2710	−0.0040	−0.0003
3	2*E*	318.16	−0.0407	0.0069	0.0022
4	3*A*	308.08	−0.0036	0.0000	0.0000
5	4*A*	292.81	−0.0195	−0.0133	0.0029
6	3*E*	286.64	0.0227	0.0063	0.0002
7	4*E*	277.08	0.1053	0.0394	−0.0076
8	5*A*	271.58	0.0246	−0.0043	0.0019
9	5*E*	269.96	0.0279	0.0042	0.0047
10	6*A*	268.27	−0.0001	0.0001	0.0000
11	7*A*	259.13	−0.0011	−0.0001	−0.0000
12	6*E*	251.17	0.0478	−0.0277	0.0098
13	7*E*	189.67	−0.0694	−0.0184	0.0057
14	8*A*	185.73	−0.0104	0.0146	0.0159
15	8*E*	185.31	0.0144	0.0028	0.0007
16	9*A*	184.31	0.0349	0.0013	0.0047
17	10*A*	180.41	−0.0020	−0.0019	0.0014

by Figures 6 and 8. Therefore, it is possible to get a set of *mean* parameters and excitation energies to simulate all of the CD spectra of the three kinds of chelates, including those conformers that have not been treated above. This has been done by utilizing the selection rules for C_3 symmetry for simplicity. The results are listed in Table 4 and also displayed in Figure 8d.

With the set of mean parameters, all CD spectra of the 16 diasteroisomers can be well reproduced by simply combining the contributions of chiral arrays involved in the conformers, regardless of their symmetries (they must be of course chiral symmetries). To further check the applicability of the parameters, some additional conformers have been also simulated, and the results are also in good agreement with those obtained at the TDDFT level. Two arbitrarily selected examples for the mixed conformers $C_1\Delta(R_eR_eS_e)(\lambda\lambda\delta)$ and $C_1\Delta(R_aR_eS_e)(\lambda\delta\delta)$ of $Ru[(pn)_3]^{2+}$ are shown in Figures 9. This result not only reveals the merit of the parameters $\underline{\Delta}$, $\underline{\delta}$ and $\underline{R}$ for *factorization* of the optical activity of these chelates, but also demonstrates the possibility of predicting the CD spectrum of a molecule according to its chiral arrays.

Conclusions

In this work we have presented a theoretical analysis for the individual contributions of the chiral arrays, Δ/Λ octahedral core, δ/λ twists of the ligand rings, and *R*/*S* chiral carbons to the CD effects of the divalent ruthenium chelates $[Ru(en)_3]^{2+}$, $[Ru(pn)_3]^{2+}$, and $[Ru(bn)_3]^{2+}$. The corresponding chiral parameters $\underline{\Delta}$, $\underline{\delta}$, and $\underline{R}$ of related transitions have been obtained and proved to be valuable for the factorization of the optical activity of these chelates.

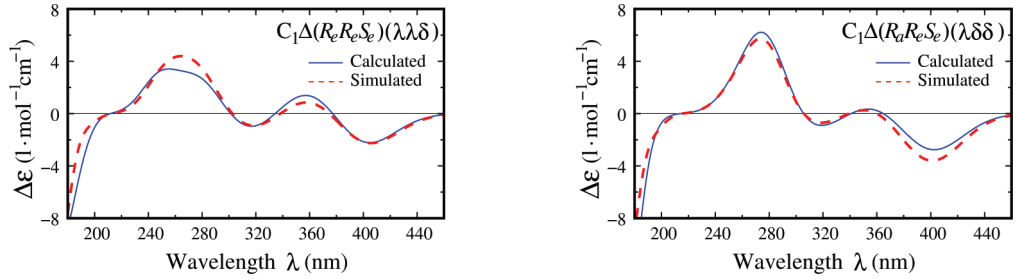

Figure 9. Comparisons of the CD curves: dotted lines are simulated curves using the mean parameters listed in Table 4, and solid lines are calculated at the TDDFT/B3LYP/LanL2DZ+6-31G* level.

We have learned the following concerning the CD effects of these chelates: (1) The three chiral arrays, Δ, δ, and *S*, each make their contributions to the CD spectra of the chelates with the sign pattern of negative, positive, negative, etc., from long wavelength to short, but the wavelengths and magnitudes of the extrema are different for different chiral arrays. (2) All CD spectra of the chelates can be well reproduced or predicted by simply combining the contributions of related chiral arrays. (3) The dominant contributions to the CD curves of the chelates arise from the influence of the Δ/Λ core configurations and less so from the δ/λ twists of the three five-membered ligand rings, while the contributions of any *R*/*S* chiral carbon atoms are small.

In addition, a Boltzmann-weighted statistical analysis shows that besides the most stable conformer $D_3\Lambda(\delta\delta\delta/lel_3)$, the less stable isomers $C_2\Lambda(\delta\delta\lambda/lel_2ob)$ and $C_2\Lambda(\delta\lambda\lambda/lelob_2)$ also make considerable contributions to the experimental CD spectrum of the $[Ru(en)_3]\cdot I_2$ chelate.

These findings not only make it possible to directly determine the absolute configurations of related chelates in solution from their CD data but also provide a deep insight into the chiroptical properties of the chelates.

Acknowledgment. This research has been supported by the National Natural Science Foundation of China (Grant No. 20673069) and by the Natural Science Foundation of Shanxi province (Grant No. 2007011021). We are indebted to Professor Robert W. Woody (Department of Biochemistry and Molecular Biology, Colorado State University, Fort Collins) for critically reading the manuscript.

Supporting Information Available: Optimized geometries, Kohn−Sham orbitals, excitation energies, oscillator and rotational strengths, as well as the chiral parameters $\underline{\Delta}$, $\underline{\delta}$, and $\underline{R}$ of related transitions for the tris-diamine ruthenium chelates reported in the present work; complete ref 21. This material is available free of charge via the Internet at http://pubs.acs.org.

JA9004738